

Regulation of membrane scission in yeast endocytosis

Deepikaa Menon¹ and Marko Kaksonen^{1*}

*For correspondence:
Marko.Kaksonen@unige.ch

¹Department of Biochemistry, University of Geneva, Geneva, Switzerland

Abstract

Introduction

Clathrin-mediated endocytosis (CME) is an endocytic process by which cargo from the cell exterior is incorporated into a Clathrin-coated vesicle that is then transported into the cell (*Bitsikas et al., 2014*). Over 50 different proteins are involved in reshaping a flat plasma membrane into an invagination that eventually separates from the membrane to form a vesicle (*Kaksonen and Roux, 2018*). In yeast, CME is the only pathway for uptake of cargo, and involves a similar membrane transformation as in other eukaryotes. Most mammalian CME proteins have homologues in yeast; these proteins establish endocytic sites and form the mechanical link between membrane and actin proteins (*Kaksonen and Roux, 2018*). Actin proteins nucleate and polymerize a branched actin network, producing the forces that bend the membrane into the stereotypical tubular invaginations seen in yeast (*Kübler et al., 1993; Kaksonen et al., 2003*). Forces that drive the final transition from tubular invagination to spherical vesicle in multicellular eukaryotes are provided by the GTPase Dynamin (*Grigliatti et al., 1973; Sweitzer and Hinshaw, 1998; Ferguson et al., 2007; Takei et al., 1995; Galli et al., 2017*). Dynamin is now known to interact via its proline-rich domain with the SH3 domains of crescent-shaped N-BAR proteins like Endophilin and Amphiphysin (*Grabs et al., 1997; Cestra et al., 1999; Farsad et al., 2001; Ferguson et al., 2009; Meinecke et al., 2013*). Conformation changes of Dynamin recruited to N-BAR molecules cause constriction of the underlying invaginated membrane, resulting in vesicle formation (*Shupliakov et al., 1997; Zhang and Hinshaw, 2001; Zhao et al., 2016*).

Yeast dynamin-like protein Vps1 has a major role in several membrane trafficking pathways (*Rothman et al., 1990; Peters et al., 2004; Hoepfner et al., 2001*), and been proposed to interact with endocytic proteins (*Nannapaneni et al., 2010; Yu and Cai, 2004; Smaczynska-de Rooij et al., 2012*). Others have failed to observe Vps1 at endocytic sites (*Goud Gadila et al., 2017; Kishimoto et al., 2011*), so the role of Vps1 in CME remains debated. In yeast cells, what then causes membrane scission is thus unclear, although some components of a scission mechanism have been identified, like the yeast N-BAR Rvs complex (*Munn et al., 1995; Kaksonen et al., 2005; D'Hondt et al., 2000; Kishimoto et al., 2011*). The Rvs complex (Rvs) is heterodimeric complex of the proteins Rvs161 and Rvs167. The two Rvs proteins are homologues of N-BAR proteins Amphiphysin and Endophilin (*Friesen et al., 2006; Youn et al., 2010*). Deletion of Rvs167 reduces scission efficiency by nearly 30% and reduces the invagination lengths at which scission occurs (*Kaksonen et al., 2005; Kukulski et al., 2012*). Apart from the canonical N-BAR domain which forms a crescent-shaped structure, Rvs167 has a Glycine-Proline-Alanine rich (GPA) region and a C-terminal SH3 domain (*Sivadon et al., 1997*). The GPA region is thought to act as a linker with no other known function, while loss of

43 the SH3 domain affects budding pattern and actin morphology (*Sivadon et al., 1997*). Most Rvs
44 deletion phenotypes can be rescued by expression of the BAR domains alone (*Sivadon et al., 1997*),
45 suggesting that the BAR domains are the functional unit of the Rvs complex.

46 The Rvs complex can tubulate liposomes in vitro, indicating that their BAR domains can impose
47 curvature on membranes (*Youn et al., 2010*). However, Rvs arrives at endocytic sites when mem-
48 brane tubes are already formed: curvature sensing rather than generation is the likely interaction of
49 the complex with endocytic sites (*Kukulski et al., 2012; Picco et al., 2015*). Rvs molecules arrive at
50 endocytic sites a few seconds before scission, and disassemble rapidly at the time of scission (*Picco*
51 *et al., 2015*), consistent with a role in vesicle formation. While it is shown to be involved in the last
52 stages of endocytosis, a mechanistic understanding of the influence of Rvs on scission remains
53 incomplete.

54 In this work we test several previously proposed scission models that allow a major role for
55 Rvs. Although the yeast Dynamin Vps1 lacks a canonical BAR-protein binding site (*Bui et al.,*
56 *2012; Moustaq et al., 2016*), it may be recruited via a different mechanism and induce scission.
57 Synaptojanins may selectively hydrolyze lipids at endocytic sites, causing line tension between two
58 lipid types that results in scission (*Liu et al., 2009*). Protein friction generated along the membrane
59 invagination has been proposed as a mechanism by which scission may occur (*Simunovic et al.,*
60 *2017*). We used quantitative live-cell imaging and genetic manipulation in *Saccharomyces cerevisiae* to
61 test these theories and investigate the function of Rvs in endocytosis. We found that Rvs is recruited
62 to endocytic sites by both BAR and SH3 domains. Of several potential actin-interacting binding
63 partners of the SH3 domains such as Myo3, Myo5, Vrp1, Abp1 (*Lila and Drubin, 1997; Colwill et al.,*
64 *1999; Madania et al., 1999; Liu et al., 2009*), we found that type I myosin Myo3 interacts with Rvs
65 SH3 domains. Our data also suggests that the aforementioned theories of membrane scission are
66 unlikely to sever the membrane in yeast, and that the forces required for scission are generated by
67 the actin network.

69 Results

70 **Rvs167, rather than Vps1 influences coat movement**

71 Yeast Dynamin-like protein Vps1 does not contain a proline-rich domain, which in mammalian cells
72 is required for recruitment to endocytic sites (*Grabs et al., 1997; Cestra et al., 1999; Farsad et al.,*
73 *2001; Meinecke et al., 2013*). In spite of the lack of a stereotypical interaction domain, some works
74 have reported its recruitment to endocytic proteins, including to N-BAR protein Rvs167 (*Yu and*
75 *Cai, 2004; Nannapaneni et al., 2010; Rooij et al., 2010*). The question of whether or not Vps1 has a
76 function at endocytic sites has been obfuscated by potential tagging-induced dysfunction of Vps1
77 molecules. Vps1 tagged both N- and C-terminally with GFP constructs failed to co-localize with
78 endocytic protein Abp1 in our hands, consistent with other work that observed localization only
79 with other parts of the trafficking pathway (*Goud Gadila et al., 2017*). We argued that even if tagging
80 Vps1 induced defects in its localization and/or function, its contribution to endocytosis could be
81 examined by observing the dynamics of other endocytic proteins in cells lacking Vps1. The canonical
82 interaction partner of Vps1, Rvs167, localizes to endocytic sites and influences scission efficiency,
83 although its exact role is unclear (*Kukulski et al., 2012; Picco et al., 2015*). In order to determine
84 the roles of these proteins in endocytic scission, we studied cells lacking Vps1 and Rvs167, and
85 compared against wild-type (WT) cells (Fig.1A-C).

86
87 Vps1 deletion was confirmed by sequencing the gene locus, and these cells also showed a previously
88 reported (*Rothman and Stevens, 1986*) growth phenotype at high temperatures (Fig.S1). Scission
89 efficiency was quantified by tracking the endocytic coat protein Sla1 tagged at the C-terminus with
90 eGFP (Fig.1C). Upon actin polymerization, the endocytic coat moves into the cytoplasm along with
91 the membrane as it invaginates (*Skruzny et al., 2012*). Movement of coat protein Sla1 thus acts as a

proxy for the growth of the plasma membrane invagination. Membrane retraction, that is, inward movement and subsequent retraction of the invaginated membrane back towards the cell wall is a scission-specific phenotype (*Kaksonen et al., 2005*). Retraction rates do not significantly increase in *vps1Δ* cells compared to the WT (Fig.1B).

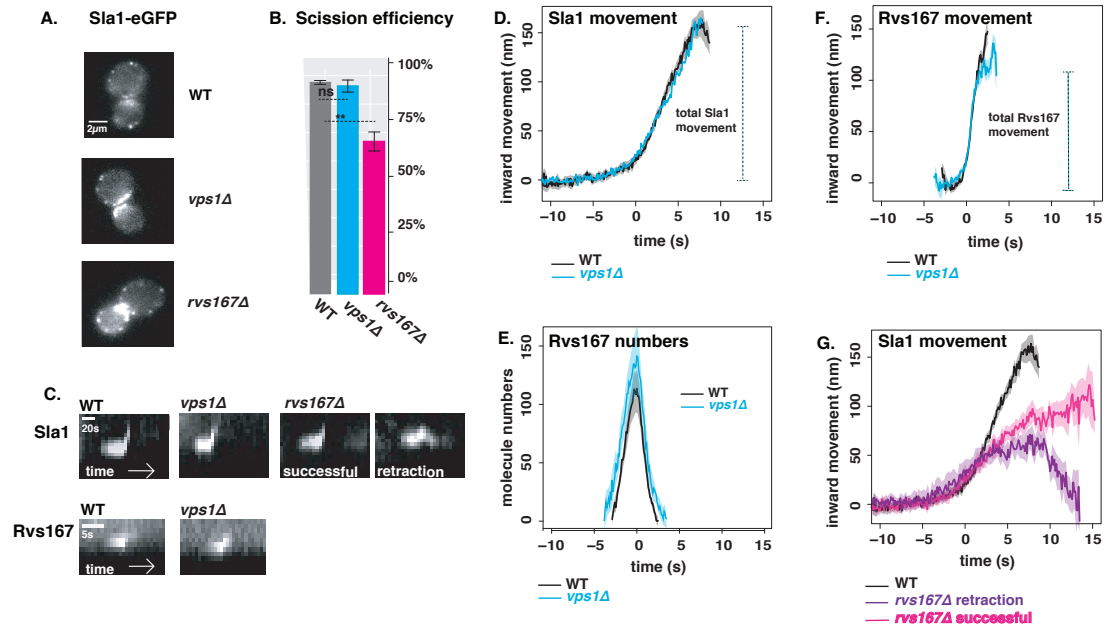


Figure 1. *vps1Δ* and *rvs167Δ* deletion **A:** Single slices from time-lapse movies of WT, *vps1Δ*, and *rvs167Δ* cells expressing Sla1-eGFP. **B:** Scission efficiency in WT, *vps1Δ*, and *rvs167Δ* cells. Error bars are standard deviation, p values from t-test, * = $p \leq 0.05$, ** = $p \leq 0.01$, *** = $p \leq 0.001$. **C:** Representative kymographs of Sla1-eGFP and Rvs167-eGFP patches in WT, *vps1Δ*, and *rvs167Δ* cells from time-lapse movies. **D:** Averaged centroid positions of Sla1-eGFP in WT and *vps1Δ* cells. **E:** Number of Rvs167 molecules in WT and *vps1Δ* cells. **F:** Averaged centroid positions of Rvs167-eGFP in WT and *vps1Δ* cells. **G:** Averaged centroid positions of Sla1-eGFP in WT, and successful and retracted Sla1-eGFP positions in *rvs167Δ* cells. All averaged positions were aligned in x axis to begin movement at time=0(s), and aligned in the y axis to a starting position = 0(nm). Shading on plots show 95% confidence intervals

The total movement of the endocytic coat (Fig.1C,D) gives an indication of when the invagination undergoes scission: greater movement would imply defects in the scission mechanism. In order to study this movement, the averaged centroid trajectory of about 50 Sla1-eGFP patches in *vps1Δ* and WT cells were tracked and compared (Fig.1D). In brief: yeast cells expressing fluorescently-tagged endocytic proteins were imaged at the equatorial plane. Since membrane invagination progresses perpendicularly to the plane of the plasma membrane, proteins that move into the cytoplasm during invagination do so in the imaging plane. Centroids of Sla1 patches- each patch being an endocytic site- were tracked in time and averaged. This provided an averaged centroid that could be followed with high spatial and temporal precision (*Picco et al., 2015*). Averaged centroid movement of Sla1-eGFP in WT cells was linear to about 140nm (Fig.1D). Sla1 movement in *vps1Δ* cells had the same magnitude of movement as WT(Fig.1D). The total movement- and so the depth of endocytic invagination - is similar to WT.

Centroid tracking has shown that the number of molecules of Rvs167 peaks at the time of scission, and is followed by a rapid loss of fluorescent intensity, simultaneous with a sharp jump of the centroid into the cytoplasm (Fig.1E,F), (*Picco et al., 2015*). This jump, also seen in Rvs167-GFP kymographs (Fig.1C), is interpreted as loss of protein on the membrane tube, causing an apparent

114 spatial jump of the centroid to protein localized at the base of the newly formed vesicle. Number of
115 molecules of Rvs167 recruited to endocytic sites in *vps1Δ* cells is not significantly different from
116 that recruited to WT cells (Fig.1E). Kymographs of Rvs167-GFP (Fig.1C), as well as Rvs167 centroid
117 tracking (Fig.1F) in *vps1Δ* cells showed the same jump as in WT.

118
119 The Rvs complex is composed of Rvs161 and Rvs167 dimers (?) so deletion of Rvs167 effectively
120 removes both proteins from endocytic sites. We quantified the effect of *rvs167Δ* on membrane
121 invagination (Fig.1A-C,G). Only 73% of Sla1 patches undergo successful scission in *rvs167Δ* cells
122 (Fig.1B). Similar scission rates have been measured in other experiments (*Kaksonen et al., 2005*)
123 and suggest failed scission in the remaining 27% of endocytic events. Coat movement both of
124 retractions and of successful endocytic events were quantified (Fig.1G) as described earlier. Sla1
125 centroid movement in both successful and retracting endocytic events in *rvs167Δ* cells look similar
126 to WT up to about 50nm (Fig.1G). In WT cells, Abp1 intensity begins to drop at scission time (Fig.S2).
127 Similarly, in successful endocytic events, Abp1 intensity drops after Sla1 centroid has moved about
128 100nm suggesting that scission occurs at invagination lengths between 60 -100 nm (Fig.S4). That
129 membrane scission occurs at shorter invagination lengths than in WT is corroborated by the smaller
130 vesicles formed in *rvs167Δ* cells by Correlative light and electron microscopy (CLEM) (*Kukulski et al.,*
131 **2012**). CLEM has moreover shown that Rvs167 localizes to endocytic sites after the invaginations
132 are about 60nm long (*Kukulski et al., 2012*). Sla1 movement in *rvs167Δ* indicates therefore that
133 membrane invagination is unaffected till Rvs is supposed to arrive.

134 **Synaptojanins likely influence vesicle uncoating, but not scission dynamics.**

135 As Vps1 did not appear to influence membrane scission, we proceeded to test another scission
136 model. The lipid hydrolysis model proposes that deletion of yeast synaptojanins would inhibit
137 scission, which would result in longer invaginations (*Liu et al., 2009*). Three Synaptojanin-like
138 proteins have been identified in *S. cerevisiae*: Inp51, Inp52, and Inp53. Inp51-eGFP exhibits a diffuse
139 cytoplasmic signal, Inp52-eGFP localizes to cortical patches that are endocytic sites and Inp53
140 localizes to patches within the cytoplasm (Fig.2A). Since Inp52 localizes to endocytic sites, we began
141 with determining the spatial and temporal recruitment of Inp52 within the endocytic machinery. We
142 aligned the averaged centroid of Inp52 in space and time to other endocytic proteins (*Picco et al.,*
143 **2015**). In order to do this, we imaged Inp52-eGFP simultaneously with Abp1-mCherry, and did the
144 same with Sla1-eGFP and Rvs167-eGFP. Using Abp1 as the common reference frame, we were able
145 to compare the arrival of the different proteins with respect to that of Abp1. We assigned as time
146 =0 (s) the fluorescent intensity maximum of Abp1, which in WT cells is concomitant with membrane
147 scission, and also coincides with the maximum of the Rvs167 fluorescent intensity (S2). On the
148 y axis, 0 (nm) indicates the position of the Sla1 centroid; positions of the other centroids are in
149 relation to the Sla1 centroid. Inp52 molecules arrived in the late stage of endocytosis after Rvs167
150 arrival, and localized to the invagination tip, suggesting a potential role in membrane scission
151 (Fig.2B).

152 Inp53 was not investigated further, as its localization conformed with other literature that found
153 that it is involved in the golgi trafficking pathway and not endocytosis (*Bensen et al., 2000*). Although
154 we were unable to observe localization of Inp51 at endocytic sites, deletion of Inp51 has been
155 shown to exacerbate the effect of *inp52Δ* on membrane retraction (*Liu et al., 2009*), so both Inp51
156 and Inp52 were tested as potential scission regulators.

157
158
159 Dynamics of Sla1-eGFP and Rvs167-eGFP in *inp51Δ* and *inp52Δ* cells were compared against the
160 WT (Fig.2C-E). Scission efficiency did not significantly decrease in *inp51Δ* compared to the WT, but
161 showed a slight decrease in *inp52Δ* cells (Fig.2C). Total movement of Sla1 and Rvs167 centroids in
162 successful endocytic events in *inp51Δ* were the same as in WT (Fig.2 D,E), while Rvs167 assembly
163 and disassembly took longer (Fig.S5). Rvs167 centroid in *inp51Δ* cells appeared to persist after

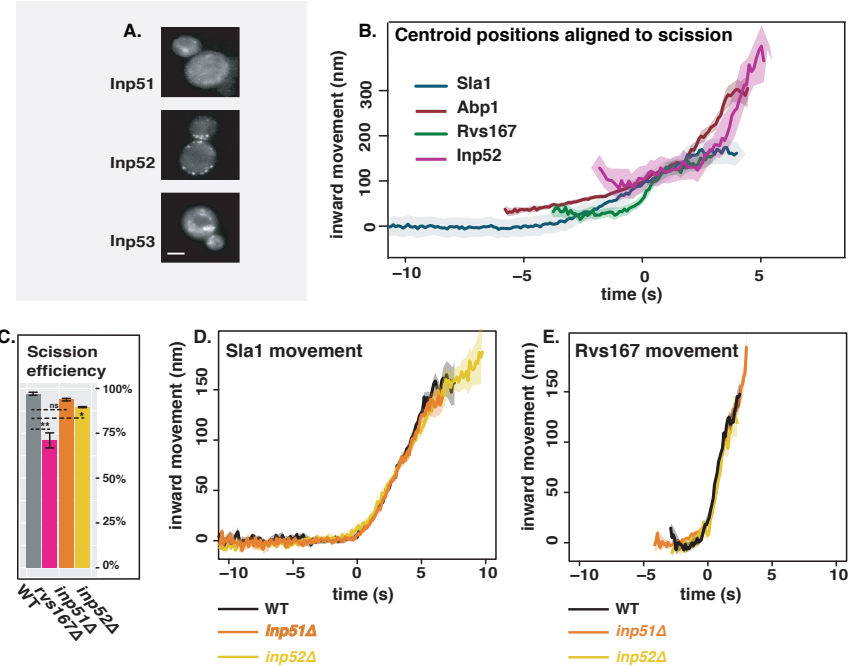


Figure 2. Involvement of yeast Synaptojanin-like proteins in endocytosis **A:** Cells endogenously tagged with Inp51-, Inp52-, and Inp53-eGFP. Scale bar = 2 μ m. **B:** Inp52 centroid trajectory was aligned in space and time to other endocytic proteins. **C:** Sla1 retraction rates in *inp51Δ* and *inp52Δ* cells compared to WT and *rvs167Δ*. Error bars are standard deviation, with p values from t-test, * = $p \leq 0.05$, ** = $p \leq 0.01$, *** = $p \leq 0.001$. **D:** Averaged centroid positions of Sla1-eGFP in WT, *inp51Δ*, and *inp52Δ* cells. **E:** Averaged centroid positions of Rvs167-eGFP in WT, *inp51Δ*, and *inp52Δ* cells. Shading on plots represent 95% confidence interval

movement compared to the WT, likely because of a delay in Rvs167 disassembly from the newly formed vesicle. In *inp52Δ* cells, Sla1 movement had the same magnitude and rate as in WT, but Sla1-eGFP signal is persistent after inward movement scission (Fig.2D). Rvs167 and Sla1 disassembly were aberrant in *inp52Δ* cells compared to WT (Fig.S5). This data are consistent with Synaptojanin involvement in assembly and disassembly of coat and scission proteins at endocytic sites rather than in membrane scission.

Rvs BAR domains recognize membrane curvature in-vivo

So far Rvs167 remains the protein that has a major influence on scission efficiency and movement of Sla1. Rvs can tubulate liposomes in vitro (Youn et al., 2010), but its interaction with membrane curvature in vivo has not so far been tested. Recruitment of the Rvs complex to endocytic sites, and BAR-membrane interaction was thus investigated further. The SH3 domain has known interactions with proteins within the actin network (Lila and Drubin, 1997; Colwill et al., 1999; Madania et al., 1999; Liu et al., 2009). We removed the contribution of the SH3 by deleting the domain (Fig.3A) and observed the localization of Rvs167 $\Delta sh3$ compared to full-length Rvs167. Endogenously tagged Rvs167-eGFP and Rvs167 $\Delta sh3$ -eGFP colocalization with Abp1-mCherry in WT and *sla2Δ* cells were compared to test if Rvs could be recruited to endocytic sites without the SH3 domain (Fig.3B). Sla2 acts as the molecular linker between forces exerted by the actin network and the plasma membrane (Skruzny et al., 2012). *sla2Δ* cells therefore contain a polymerizing actin network at endocytic patches, but the membrane has no curvature, and endocytosis fails. In these cells, the full-length Rvs167 co-localizes with Abp1-mCherry, indicating that it is recruited to endocytic sites independently of membrane curvature (Fig.3B, “*sla2Δ*”). Rvs167 $\Delta sh3$ does not appear at the plasma membrane except for rare transient patches that do not co-localize with Abp1-mCherry: Rvs167 $\Delta sh3$, that is, the BAR domain, is not recruited to endocytic sites in the absence of curvature

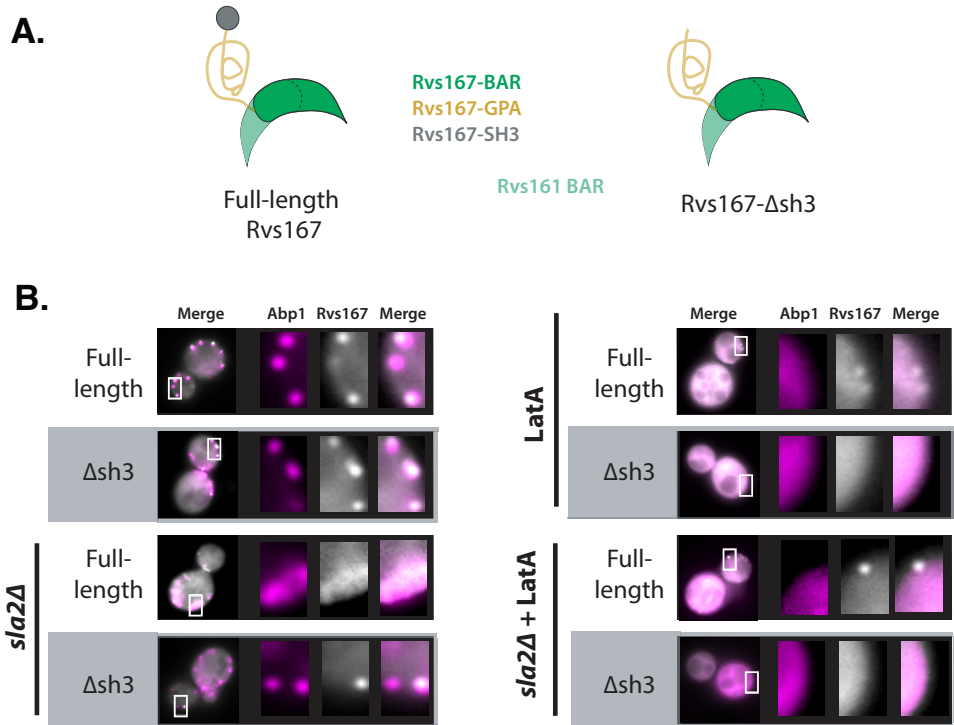


Figure 3. Localization of Rvs167 BAR domain **A:** Schematic of Rvs protein complex with and without the SH3 domain. **B:** Localization of full-length Rvs167 and Rvs167 Δ sh3 in WT, *sla2Δ*, *LatA* treated, and *LatA* treated *sла2Δ* cells. Scale bar=2 μ m.

187 in *sла2Δ* cells.

188 **Rvs SH3 domains have an actin and curvature independent localisation**

189 In order to test if genetic interactions of SH3 domains are prevalent in in vivo endocytosis, we
 190 tested the localization of Rvs167 and Rvs167 Δ sh3 in *LatA* treated cells (Fig.3B, "LatA"). Plasma
 191 membrane localization of Rvs167 remains upon *LatA* treatment, and transient patches continue
 192 to exist in *sла2Δ* cells treated with *LatA* (Fig3B, "*sла2Δ+ LatA*"). Rvs167 Δ sh3 does not localize to the
 193 plasma membrane in either case. Thus, localization of full-length Rvs167 in the presence of *LatA* is
 194 due to the SH3 domain. This indicates that the SH3 domain is able to recruit Rvs molecules to the
 195 plasma membrane in an actin- and curvature-independent manner.

196 **SH3 domains are likely recruited by Myosin 3**

197 Type I myosins Myo3 and Myo5, and Vrp1 have known genetic and/or physical interactions with
 198 Rvs167 SH3 domains (*Lila and Drubin, 1997; Colwill et al., 1999; Madania et al., 1999; Liu et al.,*
 199 *2009*). We tested the interaction between these proteins and the Rvs167 SH3 region by studying the
 200 localization of full-length Rvs167 in cells with the gene for one of these proteins deleted, and treated
 201 with *LatA*. By using *LatA* we expected to reproduce the situation in which BAR-curvature interaction
 202 is removed (Fig.4). Then, if we lost SH3 interaction because we removed the protein with which it
 203 interacts, we would lose localization of Rvs167 completely. Deletion of neither Vrp1 nor Myo5 in
 204 combination with *LatA* treatment removes the localization of Rvs167. Deletion of Myo3 with *LatA*
 205 treatment removes localization of Rvs167, indicating that SH3 domains interact at endocytic sites
 206 with Myo3.

Rvs167-eGFP

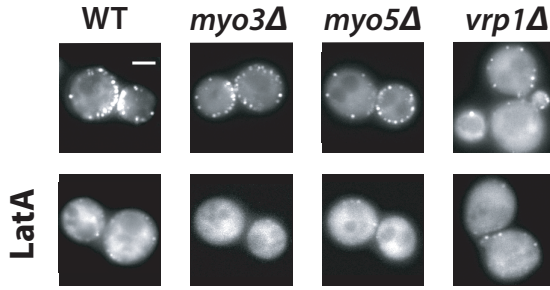


Figure 4. Localization of the SH3 domain Localization of full-length Rvs167-eGFP in WT, *myo3Δ*, *myo5Δ*, and *vrp1Δ* cells. Scale bar=2μm.

207 Loss of Rvs167 SH3 domain affects coat and actin dynamics

208 Since the Rvs167 SH3 domain has an influence on the recruitment of the Rvs complex to endocytic
209 sites, we wondered if the domain also affects later stages of invagination formation. We compared
210 dynamics of coat and scission markers in WT and *rvs167Δsh3* cells (Fig.5).

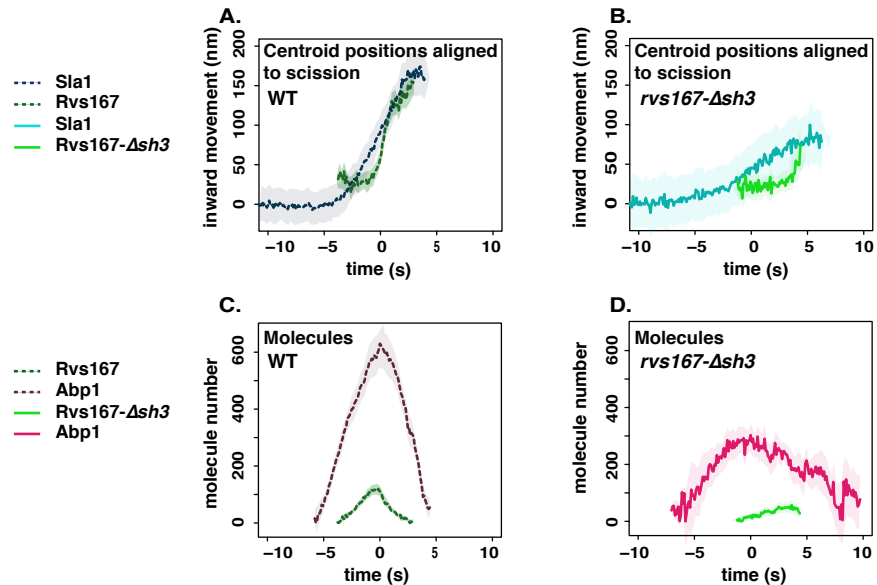


Figure 5. Endocytic dynamics in *rvs167Δsh3* cells **A,B:** Averaged centroid positions aligned in x axis so that time=0(s) is the peak of fluorescent intensity of Abp1 in respective strains. Centroids are aligned in y axis so that Sla1 begins at y=0 (nm), and Rvs167 and Rvs167 Δ sh3 positions are determined with respect to Sla1 centroids. **C,D:** Numbers of molecules in WT and *rvs167Δsh3* cells, aligned so that time=0(s) is the maximum of fluorescent intensity of Abp1 in the corresponding strains. Shading represents 95% confidence interval

211 Movement of Sla1 centroid is slower and reduced in *rvs167Δsh3* cells compared to WT (Fig.5A,B).
212 The movement of Rvs167 Δ sh3 centroid is smaller than that of full-length Rvs167 (Fig.5A,B), also
213 consistent with the formation of shorter invaginations suggested by the reduced Sla1 movement in
214 *rvs167Δsh3* cells.

215 There is delay in Rvs167 Δ sh3 recruitment compared to the onset of Abp1 assembly in *rvs167Δsh3*
216 cells compared to WT (Fig.5 C,D). In WT cells, Rvs167 and Abp1 molecule number peaks are also co-

217 incident: the actin network begins disassembling as soon as scission occurs (Fig.5C). Asynchronous
 218 peaks in *rvs167Δsh3* cells indicates a disruption in the feedback between actin network dynamics
 219 and membrane scission. Rvs167 Δ sh3 accumulation begins however, when Abp1 molecule num-
 220 bers in the mutant are about the same as in WT (about 300 copies, Fig.5C,D). . Both Rvs167 and
 221 Rvs167 Δ sh3 molecules arrive at endocytic sites when the Sla1 centroid is 20-30 nm away from
 222 its starting position. This would mean the endocytic coat has moved about 30 nm when both
 223 WT and mutant forms of Rvs are recruited. That Rvs167 Δ sh3 recruitment anticipates a certain
 224 growth of the invagination and amount of Abp1 suggests that the Rvs complex is recruited to a
 225 specific geometry of membrane invagination, and that Rvs167 Δ sh3 recruitment is delayed because
 226 invaginations in these cells take longer to acquire this geometry. Recruitment of Rvs167 Δ sh3 is
 227 reduced to half of Rvs167 (Fig.5C,D), although cytoplasmic concentration of both are similar (Fig.S6).
 228 Recruitment therefore is unlikely to be limited by cytoplasmic expression of the mutant protein.
 229 Abp1 disassembly is slowed down in *rvs167Δsh3* cells compared to WT, and recruitment is reduced
 230 to 50% of WT recruitment (Fig.5C,D), indicating disruption of actin network dynamics.

231 **Increased BAR domain recruitment corresponds to increased membrane move-
 232 ment**

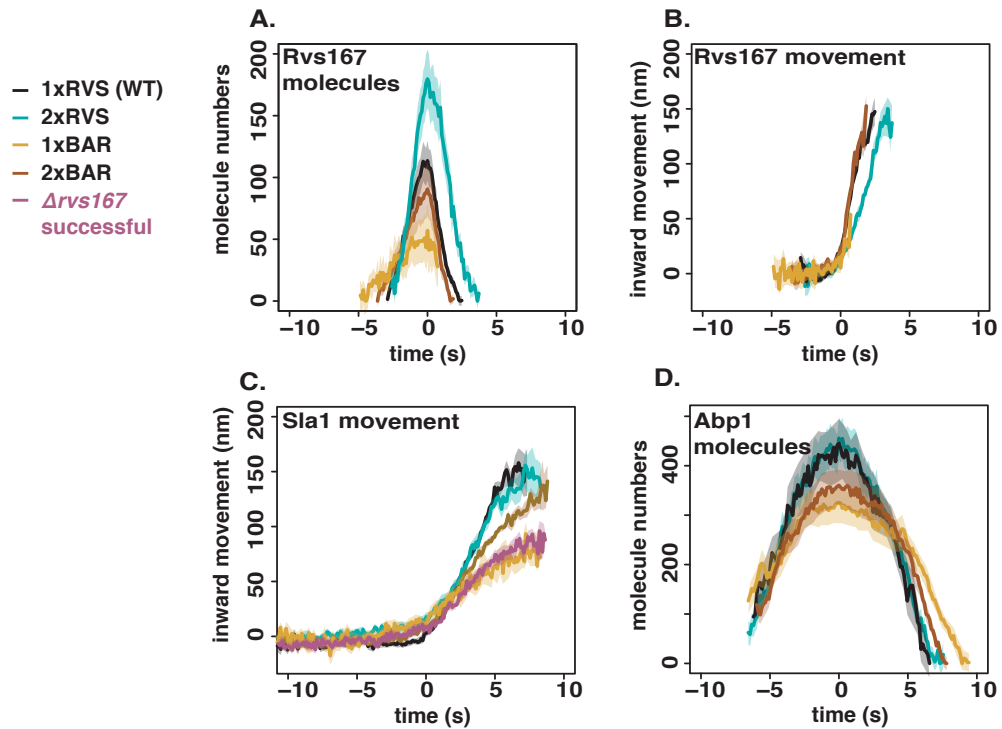


Figure 6. RVS duplication in haploid and diploid cells **A,B:** Recruitment and centroid positions of Rvs167 and Rvs167 Δ sh3 in haploid strains. **C:** Sla1 centroid positions in these strains. **D:** Abp1 recruitment in the same strains. All centroid positions were aligned in the time axis so that time=0(s) corresponds to beginning of inward movement of each average centroid. Centroids were aligned in the y axis so that y=0(nm) corresponds to the beginning of the average centroid position

233 Since removal of Rvs167 in *rvs167Δ* cells, and the reduced amount of Rvs167 Δ sh3 recruited in
 234 *rvs167Δsh3* cells results in decreased Sla1 movement, we wondered if Sla1 movement would scale
 235 with amount of Rvs recruited to endocytic sites. We titrated the amount of Rvs expressed in cells by
 236 endogenously duplicating the RVS167 and RVS161 genes (Huber et al. 2014). We also duplicated
 237 the *rvs167Δsh3* gene, resulting in cells containing 2x copies of both RVS genes (2xRVS), 1x copy of
 238 the RVS genes (1xRVS, ie WT), 2x copies of *rvs167Δsh3* (2xBAR), and 1x copy of *rvs167Δsh3* (1xBAR)

239 (Fig.6A-D).

240 Amount of WT and mutant Rvs167 molecules recruited at endocytic sites varied in these strains
241 between 50 and 180 copies (Fig.6A). "Excess" Rvs recruited to endocytic sites in the 2xRVS case does
242 not change the total movement of Rvs167 (Fig.6A,B) compared to the WT (1xRVS), although it affects
243 the disassembly dynamics. In the 2xBAR case, the amount of Rvs167 Δ sh3 molecules recruited
244 to endocytic sites increased compared to 1xBAR, as did the movement of the centroid (Fig.6B).
245 Total Abp1 numbers recruited were reduced in 1xBAR compared to the 2xBAR, 1xRVS and 2xRVS
246 (Fig.6D). Higher Abp1 numbers corresponds to larger Sla1 centroid movement (Fig.6C), indicating a
247 correlation between the maximum number of Abp1 recruited and total invagination length.

248 Discussion

249 Recruitment and function of the Rvs complex has been studied in this work, and several existing
250 models for membrane scission have been tested. We propose that Rvs is recruited to endocytic
251 sites via interactions between the Rvs BAR domains and invaginated membrane, and that SH3
252 mediated protein-protein interactions are required for efficient recruitment of Rvs. We found that
253 arrival of Rvs at the membrane invagination scaffolds the membrane and prevents membrane
254 scission. WT invagination lengths depend on recruitment of a critical number of Rvs molecules.
255 Both timing and recruitment efficiency appear crucial to Rvs function.

256 **BAR domains sense *in vivo* membrane curvature and time the recruitment of Rvs**

257 The curved structure of Endophilin and Amphiphysin BAR dimers (*Peters et al., 2004; Mim et al.,*
258 *2012*) has suggested that it may interact with curved rather than flat membranes. In the absence of
259 membrane curvature, in *sla2 Δ* cells, Rvs167 Δ sh3 domains do not localize to endocytic sites (Fig.3).
260 This demonstrates for the first time that the BAR domain senses and requires membrane curvature
261 to localize to yeast endocytic sites. Rvs167 Δ sh3 has a similar average lifetime at endocytic sites as
262 full-length Rvs167 (Fig.5C,D). However, time alignment with Abp1 shows that there is a delay in the
263 recruitment of Rvs167 Δ sh3, (Fig.5B,D). Sla1 moves inwards at a slower rate in *rvs167 Δ sh3* cells, so it
264 takes longer for the membrane in these cells to reach the same invagination length as in WT. We
265 propose that Rvs recruitment is timed to specific membrane invagination length- therefore to a
266 specific membrane curvature, accounting for the delay in recruitment. The timing of recruitment is
267 therefore provided by the BAR domain.

268 **SH3 domains allow efficient and actin independent recruitment of Rvs**

269 Rvs167 Δ sh3 accumulates to about half the WT number (Fig.5C,D), even though the same cytoplasmic
270 concentration is measured (Fig.S6), indicating that loss of the SH3 domain decreases the efficiency
271 of recruitment of Rvs. In *sla2 Δ* cells, full-length Rvs167 forms patches on the membrane (Fig.3B).
272 Since Rvs167 Δ sh3 does not localize to the plasma membrane in *sla2 Δ* cells, localization of the
273 full-length protein must be mediated by the SH3 domain. The full-length Rvs167 is able to assemble
274 and disassemble at cortical patches in *sla2 Δ* cells without the curvature- dependent interaction
275 of the BAR domain (Fig.3B). This indicates that the SH3 domain can mediate both the recruitment
276 and disassembly of Rvs at endocytic sites. In *sla2 Δ* cells treated with LatA (Fig.3B), both membrane
277 curvature and actin-interacting proteins are removed from endocytic sites. Full-length Rvs167 in
278 these cells still shows transient localizations at the plasma membrane: the SH3 domain is able to
279 localise the Rvs complex in an actin and curvature independent manner.

280 **Loss of SH3 domain disrupts endocytic actin network dynamics**

281 In WT cells, the Abp1 and Rvs167 fluorescent intensities reach maxima concomitantly (Fig.5C,D), and
282 the consequent decay of both coincide. Coincident disassembly indicates that upon vesicle scission,
283 the actin network is immediately disassembled. Membrane scission occurs around the intensity
284 peak of the two proteins (*Kukulski et al., 2012; Picco et al., 2015*). This coincident peak is lost in
285 *rvs167 Δ sh3* cells: Rvs167 Δ sh3 fluorescent intensity peaks several seconds after Abp1 intensity starts

286 to drop, and the decay of Abp1 is prolonged, taking nearly double the time as in WT. Although
287 it is not clear what the decoupling of Abp1 and Rvs167 Δ sh3 peaks means, the changes in Abp1
288 dynamics suggests a strong disruption of the actin network dynamics.

289 **Rvs acts as a membrane scaffold preventing membrane scission**

290 Invaginations in *rvs167* Δ cells undergo scission when the Sla1 centroid has moved about 80nm
291 (Fig.1F), compared to the WT lengths of 140nm. This shows that enough forces are generated at
292 80nm to cause scission. Since invagination lengths of *rvs167* Δ cells are increased by overexpression
293 of the Rvs167 Δ sh3 domains (Fig.6A-D), we think that localization of Rvs BAR domains to the mem-
294 brane tube stabilizes the membrane (*Boucrot et al., 2012; Dmitrieff and Nédélec, 2015*), increasing
295 the amount of force required to sever it. This allows the invagination to grow until WT invagination
296 lengths are acquired, and the actin network has generated enough forces to compensate for the
297 stabilization. There is a limit to the stabilization by BAR domains: in 2xRVS cells, invagination lengths
298 are the same as in 1xRVS cells even though more Rvs is recruited. It is possible that the nature of
299 the Rvs complex interaction with the membrane changes after a certain amount of Rvs is recruited,
300 since the disassembly dynamics of Rvs changes in the 2xRVS case (Fig.6A).

301 If enough forces are generated at 80nm, why is scission efficiency decreased in *rvs167* Δ com-
302 pared to WT? Forces from actin may be at a threshold when the invaginations are short. There
303 could be enough force to sever the membrane, but not enough to sever reliably. The Rvs scaffold
304 then keeps the network growing to accumulate enough actin to reliably cause scission. Controlling
305 membrane tube length could also be a way for the cell to control the size of the vesicles formed,
306 and therefore the amount of cargo packed into the vesicle.

307 **What causes membrane scission?**

308 We looked for changes in the dynamics of Sla1 and Rvs167 that would indicate a scission defect
309 in various mutant strains: longer invaginations than in WT, so Sla1 centroid movements of over
310 140nm, and a bigger inwards jump of Rvs167 centroid, indicating that a longer invagination has
311 been cut. In *vps1* Δ cells, no major changes are seen in Sla1 or Rvs167 dynamics. We conclude that
312 even if Vps1 is recruited to endocytic sites, it is not necessary for Rvs localization or function, and is
313 not necessary for scission.

314 In the lipid hydrolysis model, synaptojanins hydrolyze PIP₂ molecules that are not covered by BAR
315 domains, resulting in a boundary between hydrolyzed and non-hydrolyzed PIP₂. Interfacial forces
316 generated at this lipid boundary would then cause scission (*Liu et al., 2006*). Deleting synaptojanins
317 Inp51 and Inp52 should increase invagination lengths if scission was driven by lipid hydrolysis.
318 Sla1 and Rvs centroid dynamics shows that deletion of either Inp51 nor Inp52 result in scission
319 delay. In *inp51* Δ cells, Rvs assembly is slightly slower than that in WT: Inp51 could play a role in
320 Rvs recruitment. In the *inp52* Δ strain, about 12% of Sla1-GFP tracks retract, this could suggest
321 a moderate influence of Inp52 on scission. Rvs centroid persists after scission in *inp52* Δ cells, so
322 disassembly of Rvs after scission is delayed. Sla1 signal also persists for longer after scission in the
323 *inp52* Δ than in WT cells, suggesting that post-scission disassembly of coat proteins from the vesicle
324 is inhibited in *inp52* Δ cells. Inp52 likely plays a role in recycling endocytic proteins from the vesicle
325 to the plasma membrane.

326 The protein-friction model has proposed that BAR domains induce a frictional force on the
327 membrane, causing scission (*Simunovic et al., 2017*). If more BAR domains were added to the
328 membrane tube at a faster rate, the frictional force generated as the membrane is pulled under
329 it should increase, and the membrane should rupture faster. That is, membrane scission should
330 occur as soon as WT forces are generated on the tube. In Rvs duplicated cells, adding up to 1.6x
331 the WT amount of Rvs at faster rates to membrane tubes does not affect the length at which the
332 membrane undergoes scission (Fig.6). We think that protein friction does not contribute significantly
333 to membrane scission in yeast endocytosis.

334

335

336 In RVS duplicated cells, the maximum number of Abp1 measured is 460 ± 20 molecules. A similar
 337 amount of Abp1 is recruited in both 1xRVS and 2xRVS cases, corresponding to movement of the coat
 338 to about 140nm. We propose that recruitment of a similar amount of Abp1 before scission indicates
 339 that scission timing is dependent on the amount of Abp1, and therefore, on the amount of actin
 340 recruited. We suggest that actin supplies the forces necessary for membrane scission. The amount
 341 of force necessary is determined by the physical properties of the membrane like membrane rigidity,
 342 tension, and properties of the proteins accumulated on the membrane (**Dmitrieff and Nédélec,**
 343 **2015**). Vesicle scission releases membrane-bound Rvs, resulting in release of the SH3 along with
 344 BAR domains. Release of the SH3 domains could indicate to the actin network that vesicle scission
 345 has occurred, beginning disassembly of actin components.

346 Model for membrane scission

347 We propose that Rvs is recruited to sites by two distinct mechanisms. SH3 domains cluster Rvs at
 348 endocytic sites, increasing the efficiency with which the BAR domains sense curvature on tubular
 349 membranes. BAR domains bind to endocytic sites by sensing tubular membrane. Membrane
 350 shape is stabilized by BAR-membrane interaction against fluctuations that could cause scission.
 351 This prevent actin forces from rupturing the membrane, and the invaginations continue to grow in
 352 length as actin continues to polymerize.

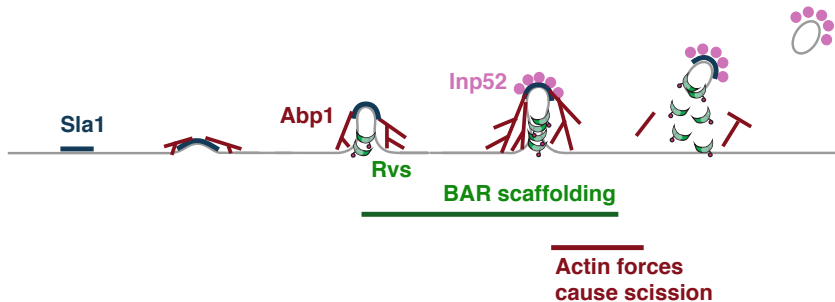


Figure 7. Model for yeast endocytic scission

353 As actin continues to polymerize, enough forces are generated to overcome the resistance to
 354 membrane scission provided by the BAR scaffold. The membrane ruptures, and vesicles are formed.
 355 Synaptojanins may help recruit Rvs at endocytic sites: Inp51 and Inp52 have proline rich regions
 356 that could act as binding sites for Rvs167 SH3 domains. They are involved in vesicle uncoating
 357 post-scission, likely by dephosphorylating PIP₂ and inducing disassembly of PIP₂-binding endocytic
 358 proteins. Eventually phosphorylation regulation allows endocytic proteins to be reused at endocytic
 359 sites, while the vesicle is transported elsewhere into the cell.

360 Methods and Materials

361 Homologous recombination with PCR cassette insertion

362 Tagging or deletion of endogenous genes was done by homologous integration of the product
 363 of a Polymerase Chain Reaction using appropriate primers and a plasmid containing a selection
 364 cassette and fluorescent tag, or only selection cassette for gene deletions. Primers were designed
 365 according to Janke et al, 2004. PCRs used the Velocity Polymerase for fluorescent tagging, and Q5
 366 for gene deletions using the NAT cassette. All fluorescently tagged genes have a C-terminus tag and
 367 are expressed endogenously. Gene deletions and fluorescent tags are checked by PCR. Vps1del and
 368 gene duplications were confirmed by sequencing.

369 **Live-cell imaging and electron microscopy**

370 Sample preparation for live imaging

371 40 μ L Concanavalin A (ConA) was incubated on a coverslip for 10 minutes. 40 μ L Yeast cells incubated
372 overnight at 25C in imaging medium SC-TRP was added to the coverslip after removing the ConA,
373 and incubated for another 10 minutes. Cells were then removed, adhered cells were washed 3x in
374 SC-TRP, and 40 μ L SC-TRP was finally added to the coverslip to prevent cells from drying.

375 Sample preparation for live imaging in LatA and sorbitol treated cells

376 Cells went through the same procedure as above till the last washing step. Instead of SC-TRP, 100x
377 diluted LatA, or Sorbitol at a final concentration of 0.2M in SC-TRP was added to the adhered cells.
378 For LatA experiments, cells were incubated in LatA for 10 minutes before imaging. For sorbitol
379 treatments, cells were imaged within 5 minutes of adding sorbitol.

380 Epifluorescent imaging for centroid tracking

381 Live-cell imaging was performed as in (*Picco et al., 2015*) Picco et al., 2015. All images were obtained
382 at room temperature using an Olympus IX81 micro-scope equipped with a 100 \times /NA 1.45 PlanApo
383 objective, with an additional 1.6x magnification lens and an EMCCD camera. The GFP channel was
384 imaged using a 470/22 nm band-pass excitation filter and a 520/35 nm band-pass emission filter.
385 mCherry epifluorescence imaging was carried out using a 556/20 nm band-pass excitation filter and
386 a 624/40 band-pass emission filter. GFP was excited using a 488 nm solid state laser and mCherry
387 was excited using a 561 nm solid state laser. Hardware was controlled using Metamorph software.
388 For single-channel images, 80-120ms was used as exposure time. All dual-channel images were
389 acquired using 250ms exposure time. Simultaneous dual-color images were obtained using a
390 dichroic mirror, with TetraSpeck beads used to correct for chromatic aberration.

391 Epifluorescent imaging for molecule number quantification

392 Images were acquired as in Picco et al., 2015. Z-stacks of cells containing the GFP-tagged protein
393 of interest, incubated along with cells containing Nuf2-GFP, were acquired using 400ms exposure
394 using a mercury vapour lamp, on a CCD camera. Z stacks were spaced at 200nm.

395 **Live-cell image analysis**

396 Images were processed for background noise using a rolling ball radius of 90 pixels. Particle
397 detection, and tracking was performed for a particle size of 6 pixels, using scripts that com-
398 bine background subtraction with Particle Tracker and Detector, that can be found on ImageJ
399 (<http://imagej.nih.gov>). Further analysis for centroid averaging, alignments between dual-color
400 images and single channel images, for alignment to the reference Abp1 were done using scripts
401 written in Matlab (Mathworks) and R (www.r-project.org), written originally by Andrea Picco, and
402 modified by me. Details of analysis can be found at (*Picco et al., 2015*). All movement and intensity
403 plots from centroid tracking show the average centroid with 95% confidence interval. All molecule
404 number quantifications report either the median or maximum number of molecules with standard
405 error of mean. Maximum number is preferred over median in cases when the rate of change of
406 fluorescent intensity of two populations being compared are not similar, and the lifetime of the
407 protein populations being compared are not similar. The median in this case underreports the
408 differences in protein accumulation.

409 **Cytoplasmic background quantification**

410 On a maximum intensity projection of time-lapse images, the average pixel intensity within a circle
411 of set radius in the cytoplasm was measured. This circle is manually arranged so that cortical
412 patches were excluded, and mean intensity was acquired for about 10 cells of each cell type. A
413 fixed area outside the cells was drawn, and mean intensity was calculated to establish "background
414 intensity". This background intensity was then subtracted from the mean intensity to obtain a

415 rough measure of cytoplasmic intensity. There are some caveats with this quantification: the cells
416 were not incubated in the same field of view, cellular autofluorescence is assumed to be equal for
417 the different strains.

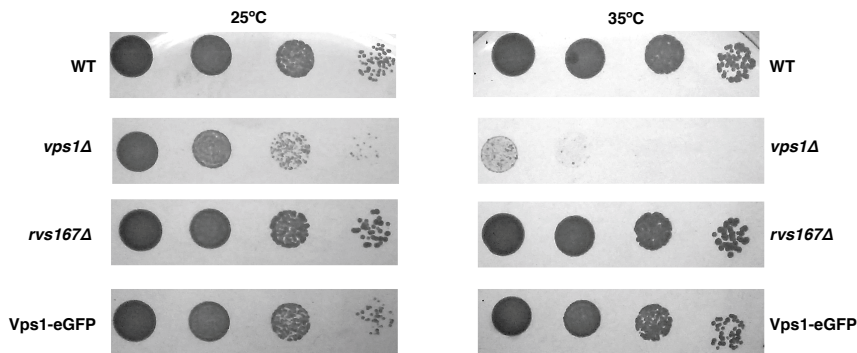
418 **References**

- 419 Bensen, E. S., Costaguta, G., and Payne, G. S. (2000). Synthetic genetic interactions with temperature-sensitive
420 clathrin in *Saccharomyces cerevisiae*. Roles for synaptojanin-like Inp53p and dynamin-related Vps1p in
421 clathrin-dependent protein sorting at the trans-Golgi network. *Genetics*, 154(1):83–97.
- 422 Bitsikas, V., Corrêa, I. R., and Nichols, B. J. (2014). Clathrin-independent pathways do not contribute significantly
423 to endocytic flux. *eLife*, 3:e03970.
- 424 Boucrot, E., Pick, A., Camdere, G., Liska, N., Evergren, E., McMahon, H. T., and Kozlov, M. M. (2012). Membrane
425 Fission Is Promoted by Insertion of Amphipathic Helices and Is Restricted by Crescent BAR Domains. *Cell*,
426 149(1):124–136.
- 427 Bui, H. T., Karren, M. A., Bhar, D., and Shaw, J. M. (2012). A novel motif in the yeast mitochondrial dynamin Dnm1
428 is essential for adaptor binding and membrane recruitment. *The Journal of cell biology*, 199(4):613–22.
- 429 Cestra, G., Castagnoli, L., Dente, L., Minenkova, O., Petrelli, A., Migone, N., Hoffmüller, U., Schneider-Mergener, J.,
430 and Cesareni, G. (1999). The SH3 domains of endophilin and amphiphysin bind to the proline-rich region of
431 synaptojanin 1 at distinct sites that display an unconventional binding specificity. *The Journal of biological
432 chemistry*, 274(45):32001–7.
- 433 Colwill, K., Field, D., Moore, L., Friesen, J., and Andrews, B. (1999). In Vivo Analysis of the Domains of Yeast Rvs167p
434 Suggests Rvs167p Function Is Mediated Through Multiple Protein Interactions. *Genetics*, 152(3):881–893.
- 435 D'Hondt, K., Heese-Peck, A., and Riezman, H. (2000). Protein and Lipid Requirements for Endocytosis. *Annual
436 Review of Genetics*, 34(1):255–295.
- 437 Dmitrieff, S. and Nédélec, F. (2015). Membrane Mechanics of Endocytosis in Cells with Turgor. *PLoS Comput Biol*,
438 11(10):e1004538.
- 439 Farsad, K., Ringstad, N., Takei, K., Floyd, S. R., Rose, K., and De Camilli, P. (2001). Generation of high curvature
440 membranes mediated by direct endophilin bilayer interactions. *The Journal of Cell Biology*, 155(2):193–200.
- 441 Ferguson, S. M., Brasnjo, G., Hayashi, M., Wölfel, M., Colles, C., Giovedi, S., Raimondi, A., Gong, L. W., Ariel, P.,
442 Paradise, S., O'Toole, E., Flavell, R., Cremona, O., Miesenböck, G., Ryan, T. A., and De Camilli, P. (2007). A selective
443 activity-dependent requirement for dynamin 1 in synaptic vesicle endocytosis. *Science*, 316(5824):570–574.
- 444 Ferguson, S. M., Raimondi, A., Paradise, S., Shen, H., Mesaki, K., Ferguson, A., Destaing, O., Ko, G., Takasaki, J.,
445 Cremona, O., O'Toole, E., and De Camilli, P. (2009). Coordinated actions of actin and BAR proteins upstream
446 of dynamin at endocytic clathrin-coated pits. *Developmental cell*, 17(6):811–822.
- 447 Friesen, H., Humphries, C., Ho, Y., Schub, O., Colwill, K., and Andrews, B. (2006). Characterization of the Yeast
448 Amphiphysins Rvs161p and Rvs167p Reveals Roles for the Rvs Heterodimer In Vivo. *Molecular Biology of the
449 Cell*, 17(3):1306–1321.
- 450 Galli, V., Sebastian, R., Moutel, S., Ecard, J., Perez, F., and Roux, A. (2017). Uncoupling of dynamin polymerization
451 and GTPase activity revealed by the conformation-specific nanobody dynab. *eLife*, 6:e25197.
- 452 Goud Gadila, S. K., Williams, M., Saimani, U., Delgado Cruz, M., Makaraci, P., Woodman, S., Short, J. C., McDermott,
453 H., and Kim, K. (2017). Yeast dynamin Vps1 associates with clathrin to facilitate vesicular trafficking and
454 controls Golgi homeostasis. *European Journal of Cell Biology*, 96(2):182–197.
- 455 Grabs, D., Slepnev, V. I., Songyang, Z., David, C., Lynch, M., Cantley, L. C., and De Camilli, P. (1997). The SH3
456 domain of amphiphysin binds the proline-rich domain of dynamin at a single site that defines a new SH3
457 binding consensus sequence. *The Journal of biological chemistry*, 272(20):13419–25.
- 458 Grigliatti, T. A., Hall, L., Rosenbluth, R., and Suzuki, D. T. (1973). Temperature-Sensitive Mutations in *Drosophila*
459 *melanogaster* XIV. A Selection of Immobile Adults *. *Molec. gen. Genet.*, 120:107–114.
- 460 Hoepfner, D., van den Berg, M., Philippse, P., Tabak, H. F., and Hettema, E. H. (2001). A role for Vps1p, actin, and
461 the Myo2p motor in peroxisome abundance and inheritance in <i>Saccharomyces cerevisiae</i>. *The Journal
462 of Cell Biology*, 155(6):979–990.

- 463 Kaksonen, M. and Roux, A. (2018). Mechanisms of clathrin-mediated endocytosis.
- 464 Kaksonen, M., Sun, Y., and Drubin, D. G. (2003). A pathway for association of receptors, adaptors, and actin
465 during endocytic internalization. *Cell*, 115(4):475–487.
- 466 Kaksonen, M., Toret, C. P., and Drubin, D. G. (2005). A modular design for the clathrin- and actin-mediated
467 endocytosis machinery. *Cell*, 123(2):305–320.
- 468 Kishimoto, T., Sun, Y., Buser, C., Liu, J., Michelot, A., and Drubin, D. G. (2011). Determinants of endocytic
469 membrane geometry, stability, and scission. *Proceedings of the National Academy of Sciences of the United
470 States of America*, 108(44):E979–E988.
- 471 Kübler, E., Riezman, H., Riezman, H., and Riezman, H. (1993). Actin and fimbrin are required for the internalization
472 step of endocytosis in yeast. *The EMBO Journal*, 12(7):2855–62.
- 473 Kukulski, W., Schorb, M., Kaksonen, M., and Briggs, J. G. (2012). Plasma Membrane Reshaping during Endocytosis
474 Is Revealed by Time-Resolved Electron Tomography. *Cell*, 150(3):508–520.
- 475 Lila, T. and Drubin, D. G. (1997). Evidence for physical and functional interactions among two *Saccharomyces
476 cerevisiae* SH3 domain proteins, an adenylyl cyclase-associated protein and the actin cytoskeleton. *Molecular
477 Biology of the Cell*, 8(2):367–385.
- 478 Liu, J., Kaksonen, M., Drubin, D. G., and Oster, G. (2006). Endocytic vesicle scission by lipid phase boundary
479 forces. *Proceedings of the National Academy of Sciences of the United States of America*, 103(27):10277–82.
- 480 Liu, J., Sun, Y., Drubin, D. G., and Oster, G. F. (2009). The Mechanochemistry of Endocytosis. *PLoS Biol*,
481 7(9):e1000204.
- 482 Madania, A., Dumoulin, P., Grava, S., Kitamoto, H., Scharer-Brodbeck, C., Soulard, A., Moreau, V., and Winsor,
483 B. (1999). The *Saccharomyces cerevisiae* Homologue of Human Wiskott-Aldrich Syndrome Protein Las17p
484 Interacts with the Arp2/3 Complex. *Molecular Biology of the Cell*, 10(10):3521–3538.
- 485 Meinecke, M., Boucrot, E., Camdere, G., Hon, W.-C., Mittal, R., and McMahon, H. T. (2013). Cooperative recruitment
486 of dynamin and BIN/amphiphysin/Rvs (BAR) domain-containing proteins leads to GTP-dependent membrane
487 scission. *The Journal of biological chemistry*, 288(9):6651–61.
- 488 Mim, C., Cui, H., Gawronski-Salerno, J. A., Frost, A., Lyman, E., Voth, G. A., and Unger, V. M. (2012). Structural
489 basis of membrane bending by the N-BAR protein endophilin. *Cell*, 149(1):137–145.
- 490 Moustaq, L., Smaczynska-de Rooij, I. I., Palmer, S. E., Marklew, C. J., and Ayscough, K. R. (2016). Insights into
491 dynamin-associated disorders through analysis of equivalent mutations in the yeast dynamin Vps1. *Microbial
492 cell (Graz, Austria)*, 3(4):147–158.
- 493 Munn, A. L., Stevenson, B. J., Gelli, M. I., and Riezman, H. (1995). end5, end6, and end7: Mutations that cause
494 actin delocalization and block the internalization step of endocytosis in *Saccharomyces cerevisiae*. *Molecular
495 Biology of the Cell*, 6(12):1721–1742.
- 496 Nannapaneni, S., Wang, D., Jain, S., Schroeder, B., Highfill, C., Reustle, L., Pittsley, D., Maysent, A., Moulder, S.,
497 McDowell, R., and Kim, K. (2010). The yeast dynamin-like protein Vps1:vps1 mutations perturb the internal-
498 ization and the motility of endocytic vesicles and endosomes via disorganization of the actin cytoskeleton.
499 *European Journal of Cell Biology*, 89(7):499–508.
- 500 Peters, C., Baars, T. L., Bühler, S., and Mayer, A. (2004). Mutual control of membrane fission and fusion proteins.
501 *Cell*, 119(5):667–78.
- 502 Picco, A., Mund, M., Ries, J., Nédélec, F., and Kaksonen, M. (2015). Visualizing the functional architecture of the
503 endocytic machinery. *eLife*, page e04535.
- 504 Rooij, I. I. S.-d., Allwood, E. G., Aghamohammazadeh, S., Hettema, E. H., Goldberg, M. W., and Ayscough,
505 K. R. (2010). A role for the dynamin-like protein Vps1 during endocytosis in yeast. *Journal of Cell Science*,
506 123(20):3496–3506.
- 507 Rothman, J. H., Raymond, C. K., Gilbert, T., O'Hara, P. J., and Stevens, T. H. (1990). A putative GTP binding protein
508 homologous to interferon-inducible Mx proteins performs an essential function in yeast protein sorting. *Cell*,
509 61(6):1063–1074.

- 510 Rothman, J. I. and Stevens, T. H. (1986). Protein Sorting in Yeast: Mutants Defective in Vacuole Biogenesis
 511 Mislocalize Vacuolar Proteins into the Late Secretory Pathway. Technical report.
- 512 Shupliakov, O., Löw, P., Grabs, D., Gad, H., Chen, H., David, C., Takei, K., De Camilli, P., and Brodin, L. (1997).
 513 Synaptic vesicle endocytosis impaired by disruption of dynamin-SH3 domain interactions. *Science (New York,*
 514 *N.Y.)*, 276(5310):259–63.
- 515 Simunovic, M., Manneville, J.-B., Renard, H.-F. O., Johannes, L., Bassereau, P., Callan, A., Correspondence, J.,
 516 Evergren, E., Raghunathan, K., Bhatia, D., Kenworthy, A. K., Voth, G. A., Prost, J., Mcmahon, H. T., and Callan-
 517 Jones, A. (2017). Friction Mediates Scission of Tubular Membranes Scaffolded by BAR Proteins. *Cell*, 170:1–13.
- 518 Sivadon, P., Crouzet, M., and Aigle, M. (1997). Functional assessment of the yeast Rvs161 and Rvs167 protein
 519 domains. *FEBS letters*, 417(1):21–27.
- 520 Skruzny, M., Brach, T., Ciuffa, R., Rybina, S., Wachsmuth, M., and Kaksonen, M. (2012). Molecular basis for
 521 coupling the plasma membrane to the actin cytoskeleton during clathrin-mediated endocytosis. *Proceedings*
 522 *of the National Academy of Sciences of the United States of America*, 109(38):E2533–42.
- 523 Smaczynska-de Rooij, I. I., Allwood, E. G., Mishra, R., Booth, W. I., Aghamohammazadeh, S., Goldberg, M. W., and
 524 Ayscough, K. R. (2012). Yeast Dynamin Vps1 and Amphiphysin Rvs167 Function Together During Endocytosis.
 525 *Traffic*, 13(2):317–328.
- 526 Sweitzer, S. M. and Hinshaw, J. E. (1998). Dynamin Undergoes a GTP-Dependent Conformational Change Causing
 527 Vesiculation. *Cell*, 93(6):1021–1029.
- 528 Takei, K., McPherson, P. S., Schmid, S. L., and Camilli, P. D. (1995). Tubular membrane invaginations coated by
 529 dynamin rings are induced by GTP- γ S in nerve terminals. *Nature*, 374(6518):186–190.
- 530 Youn, J.-Y., Friesen, H., Kishimoto, T., Henne, W. M., Kurat, C. F., Ye, W., Ceccarelli, D. F., Sicheri, F., Kohlwein, S. D.,
 531 McMahon, H. T., and Andrews, B. J. (2010). Dissecting BAR Domain Function in the Yeast Amphiphysins Rvs161
 532 and Rvs167 during Endocytosis. *Molecular Biology of the Cell*, 21(17):3054–3069.
- 533 Yu, X. and Cai, M. (2004). The yeast dynamin-related GTPase Vps1p functions in the organization of the actin
 534 cytoskeleton via interaction with Sla1p. *Journal of Cell Science*, 117(17):3839–3853.
- 535 Zhang, P. and Hinshaw, J. E. (2001). Three-dimensional reconstruction of dynamin in the constricted state. *Nature*
 536 *Cell Biology*, 3(10):922–926.
- 537 Zhao, W.-D., Hamid, E., Shin, W., Wen, P. J., Krystofiak, E. S., Villarreal, S. A., Chiang, H.-C., Kachar, B., and Wu, L.-G.
 538 (2016). Hemi-fused structure mediates and controls fusion and fission in live cells. *Nature*, 534(7608):548–52.
- 539
- 540

541 Supplementary Material



542 **Figure S1. Growth assay of WT, vps1 Δ , rvs167 Δ , and cells expressing Vps1-eGFP at 25°C and 35°C**

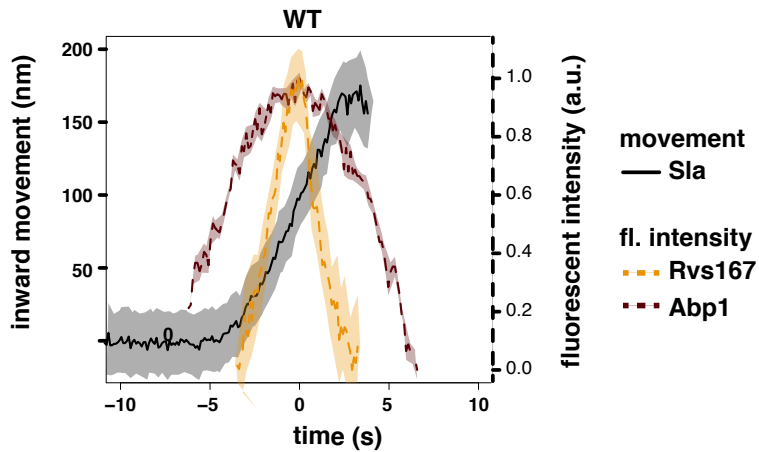


Figure S2. Sla1 centroid aligned so that time=0(s) is the maximum of Abp1 fluorescent intensity in WT cells (Picco et al., 2015), normalized Abp1 and Rvs167 fluorescent intensities in WT cells

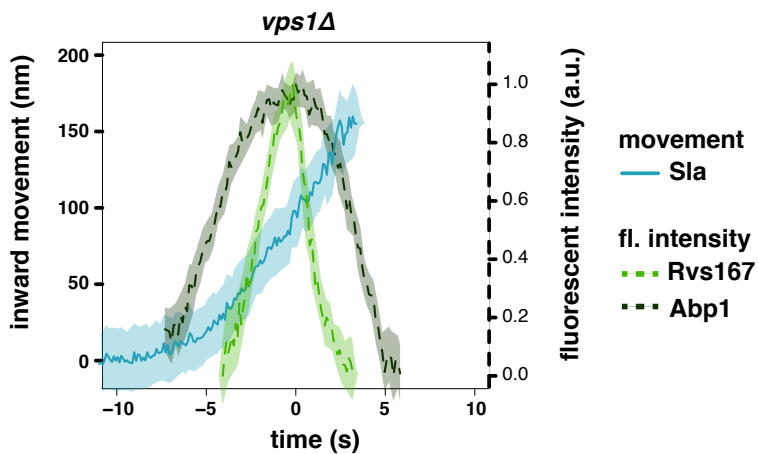


Figure S3. Sla1 centroid aligned so that time=0(s) is the maximum of Abp1 fluorescent intensity in *vps1 Δ* cells (Picco et al., 2015), normalized Abp1 and Rvs167 fluorescent intensities in *vps1 Δ* cells

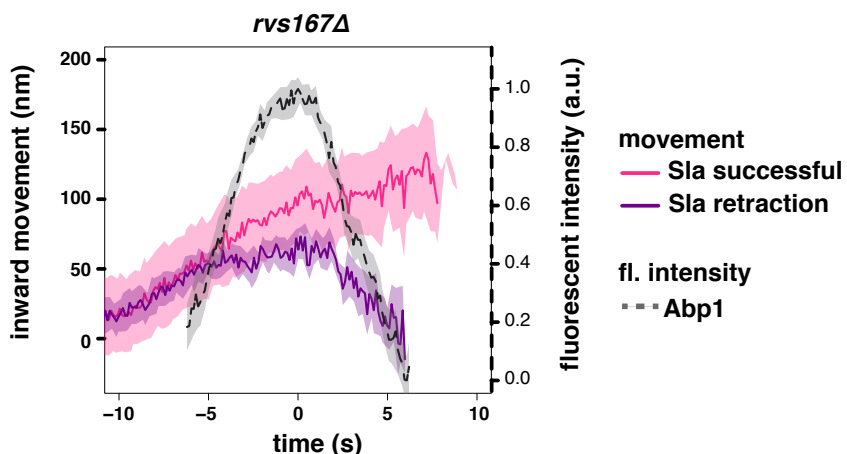


Figure S4. Sla1 centroid aligned so that time=0(s) is the maximum of Abp1 fluorescent intensity in *rvs167 Δ* cells (Picco et al., 2015), normalized Abp1 fluorescent intensity in *rvs167 Δ* cells

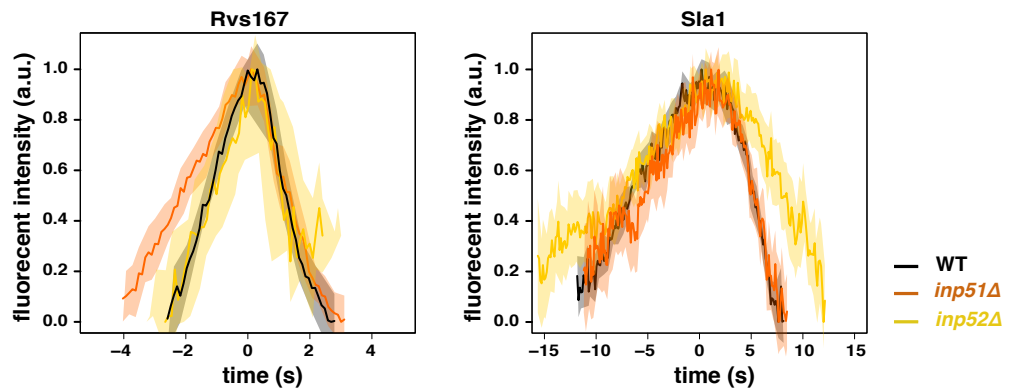


Figure S5. Normalized Rvs167 and Sla1 fluorescent intensities aligned in time so that time=0(s) is the maximum of each corresponding fluorescent intensity profile



Figure S6. Cytoplasmic intensity and intensity of endocytic patches of Rvs167 and Rvs167 Δ sh3 in WT and rvs167 Δ sh3 cells. Error bars are standard deviation, p values from t-test, * = $p \leq 0.05$, ** = $p \leq 0.01$, *** = $p \leq 0.001$.